Measurement Science
and Technology

PURPOSE-LED
PUBLISHING™

PAPER • **OPEN ACCESS**

Laplace domain dynamic calibration in city-wide sensor networks

To cite this article: Henrik Söderblom *et al* 2026 *Meas. Sci. Technol.* **37** 455108

View the article online for updates and enhancements.



This content was downloaded from IP address 32.198.60.50 on 27/11/2026 at 11:13

Measurement Science and Technology

Check for updates

PAPER

Laplace domain dynamic calibration in city-wide sensor networks

Henrik Söderblom[1,2,*], **Martha A Zaidan**[3,4], **Maitane Iturrate-Garcia**[5], **Hasan Sarwar**[3,4], **Richard Högström**[1], **Tuukka Petäjä**[4] **and Shahin Tabandeh**[1]

[1] MIKES (National Metrology Institute), VTT Technical Research Centre of Finland, Espoo, Finland
[2] Department of Science and Engineering, Åbo Akademi University, Turku, Finland
[3] Department of Computer Science, University of Helsinki, Helsinki, Finland
[4] Institute for Atmospheric and Earth System Research (INAR), University of Helsinki, Helsinki, Finland
[5] Federal Institute of Metrology METAS, Bern-Wabern, Switzerland
[*] Author to whom any correspondence should be addressed.

E-mail: henrik.soderblom@vtt.fi

Keywords: sensor network metrology, sensor networks, Laplace transform, calibration, uncertainty analysis

OPEN ACCESS

RECEIVED
3 July 2026

REVISED
16 September 2026

ACCEPTED FOR PUBLICATION
4 November 2026

PUBLISHED
13 November 2026

Original content from this work may be used under the terms of the Creative Commons Attribution 4.0 licence.

Any further distribution of this work must maintain attribution to the author(s) and the title of the work, journal citation and DOI.

Abstract

Urban sensor networks can provide spatially and temporally resolved environmental information, but their measurement trustworthiness depends on maintaining an unbroken chain of traceability to the International System of Units (SI) and on quantifying the associated uncertainties under dynamic field conditions. This paper applies a Laplace-domain method for *in situ* calibration of city-wide sensor networks under dynamic conditions, i.e. non-steady state. The method estimates pairwise dynamic relationships between sensor signals, separates a medium-related spatial effect, and solves an overdetermined calibration problem with a known network reference. Measurement uncertainty is propagated using a Monte Carlo approach. The method is evaluated using two urban datasets: a Helsinki network linked to the SMEAR III station and an Antwerp network from the SensEURCity project. Calibration coefficients were obtained for temperature, relative humidity (RH), and pressure in both networks. Particulate matter (PM_{10} and $PM_{2.5}$) calibration was feasible only under restricted sensor-subset conditions because of the localized and weakly correlated nature of PM signals. A transfer function-based malfunction indicator was also tested by introducing artificial shifts, showing that shifted measurement signals can be identified when the network geometry and signal correlations are sufficient. The results demonstrate the potential of Laplace-domain modeling as an uncertainty-aware route for dynamic calibration transfer in deployed sensor networks, while highlighting limitations related to interpolation, spatial heterogeneity, network geometry, and measurand-specific correlation.

1. Introduction

Air pollution is one of the environmental health risk factors of major concern globally causing about 6.6 million deaths per year [1]. In addition to population aging and emerging diseases, global warming poses additional health risks resulting from the synergies between air pollution and climate change, such as increasing tropospheric ozone exposure, wildfires, extreme heat, and droughts [2, 3]. Despite documented evidence on the negative effects of air pollution on human health [4–6], air pollution burden remains unknown in many regions.

Particulate matter (PM) is one of the air pollutants of major concern for public health, including risks such as respiratory and cardiovascular diseases [7–9]. The smaller the particles, the larger the negative impact on human health [7]. The World Health Organization (WHO) has estimated that only $PM_{2.5}$ alone is the cause of 100 000 deaths per year. Thus, as highlighted by WHO, monitoring ambient pollution and assessing the exposure of the population to PM is critical for tracking the effectiveness of air quality policies. However, the public's stance regarding the matter is still not on a level corresponding to the health risk [8]. It is evident that the need for suitable air quality monitoring techniques is of great importance.

© 2026 The Author(s). Published by IOP Publishing Ltd

Air quality monitoring has improved in recent years, mostly thanks to the development of advanced real-time monitoring systems, contributing to the lessened usage of traditional manual measurement techniques [8]. Development connected to the reduced size and cost of sensors has enabled more possibilities for different kinds of air quality monitoring [10, 11]. Air quality and environmental monitoring is increasingly moving from sparse networks of reference-grade stations towards denser measurement systems that combine reference instruments, research-grade devices, and lower-cost sensor nodes. Such networks can provide information with higher spatial and temporal resolution than conventional monitoring infrastructure alone, which is important for observing local gradients, transient events, and spatially heterogeneous exposure patterns in urban environments [12–14], while this kind of measurement setups also reduces the need for educated personnel familiar with operation and calibration of reference-grade stations [11]. However, increasing the number of measurement nodes does not automatically lead to better measurement information. The added value of a dense sensor network depends on whether the data are reliable, comparable, and accompanied by a meaningful statement of uncertainty, which are achieved through calibration and metrological traceability.

The metrological challenge in sensor networks is that the measurement result is produced not by an isolated instrument, but by a distributed system of sensors, data streams, calibration models, and processing steps. Sensor readings can be affected by calibration bias, cross-sensitivities, environmental influence quantities, aging, drift, local installation effects, and communication or preprocessing choices [11, 15]. For this reason, calibration and data validation cannot be treated only as occasional maintenance operations as they are part of the measurement model of the network. In particular, traceability to a reference sensor or reference station, propagation of measurement uncertainty, and detection of sensor malfunction are required if the network output is to be used as measurement information rather than only as indicative data.

Conventional laboratory calibration remains the most controlled route for establishing traceability, but it is not sufficient by itself for large deployed sensor networks. Removing many sensors from a city-scale network for periodic laboratory calibration is often impractical, costly, and disruptive. More importantly, laboratory calibration may not reproduce the dynamic and spatially varying conditions experienced by the sensors during operation. Field co-location with a reference instrument is therefore widely used for environmental sensors providing valuable calibration information under realistic conditions [16–20]. Nevertheless, co-location is usually limited to specific places and time periods. A calibration model obtained during co-location may not remain valid after deployment if the sensor experiences different environmental conditions, different pollutant mixtures, or long-term drift.

In-situ calibration and co-calibration have been proposed as practical ways to maintain calibration information during deployment [21–23]. In this context, a reference sensor, reference station, or a subset of traceably calibrated sensors can be used to provide the traceability to other nodes in the network. The difficulty is that differences between two sensor signals are not caused only by sensor calibration errors. They may also reflect real spatial and temporal variations in the measured quantity. In an urban network, two sensors can legitimately observe different values because they are exposed to different local conditions. A calibration method must therefore distinguish, as far as possible, between sensor-specific response and medium-related effects caused by spatial separation, transport, local sources, and dynamic environmental conditions.

Several data-driven approaches have been used to improve the quality of low-cost environmental sensor data, including linear and multivariate calibration, machine-learning correction, calibration transfer, virtual sensing, and sensor fusion [15, 24, 25]. These approaches have significantly improved the practical usability of dense monitoring systems. However, many of them are evaluated mainly through prediction error against a co-located or nearby reference station. From a measurement science perspective, this is not always sufficient. A calibration method should also provide interpretable calibration parameters, identify the role of the reference in the traceability chain, account for the dynamic response of the sensors and the medium, and propagate uncertainty through the network solution. This is the gap addressed in the present work.

In a previous work, we proposed and metrologically validated a Laplace-domain method for temperature calibration in a small laboratory sensor network [26] and discussed its uncertainty assessment in [27]. The central idea is to use transfer functions between sensor signals to estimate calibration coefficients associated with the asymptotic responses of the sensors, without requiring the physical system to reach steady state. This is relevant for deployed environmental networks since city-scale measurements are rarely obtained under stable or spatially uniform conditions. Instead of treating transient behavior only as a disturbance, the Laplace-domain formulation uses the dynamic relationship between sensor signals to separate, under stated assumptions, sensor-specific behavior from the medium effect between sensor locations.

To further test this method and ensure its applicability to real-world sensor networks, we have in this paper conducted a study consisting of calibrations of sensors in two different sensor networks, one located in Helsinki and one in Antwerp. In the Helsinki sensor network, the method is applied to temperature, relative humidity (RH), and pressure measurements using the SMEAR III station as the network [14, 15, 28]. In the Antwerp sensor network, part of the SensEURCity project, the method is applied to temperature, RH, pressure and, under restricted sensor-subset conditions, PM measurements [24]. These two datasets provide complementary tests of the approach; the Helsinki case includes hourly data from the sensors under calibration, and therefore, requires interpolation before transfer function estimation, whereas the Antwerp case provides one-min data from a larger urban deployment.

The contributions of this paper are fourfold. First, it demonstrates the use of a Laplace-domain dynamic calibration method on real city-scale sensor network data. Second, it estimates calibration coefficients and associated uncertainties by combining pairwise transfer functions, a fitted medium-effect model, and an overdetermined network solution linked to a reference sensor. Third, it compares the behavior of the method for spatially smoother measurands, such as temperature, RH, and pressure, with the more localized behavior of PM measurements. Fourth, it investigates whether changes in the transfer function structure can be used as an indicator of sensor drift. The aim is not to replace reference-grade monitoring or conventional calibration, but to provide an uncertainty-aware route for transferring calibration information within deployed sensor networks under dynamic field conditions.

The remainder of the paper is organized as follows. Section 2 presents the theoretical basis of the Laplace-domain calibration method and describes the Helsinki and Antwerp datasets. Section 3 introduces two transfer function-based indicators for synthetic drift and malfunction detection. Section 4 presents and discusses the calibration and drift-detection results, followed by conclusions in section 5.

2. Method

The method is based on the idea of separating the medium effect present in the signals of the sensors in a sensor network, to obtain a sensor calibration coefficient that corresponds to the intrinsic behavior of the sensors. The method obtains the pairwise transfer function between the sensor signals through the Laplace transform, from which then the medium effect can be modeled. This is followed by separating the medium effect from the transfer functions, resulting in sensor specific signals from which calibration coefficients dependent only on intrinsic sensor response can be estimated. The following subsection explains the theory briefly and a more detailed explanation can be found in [26].

2.1. Theory

The idea of using the Laplace transform on the signals of the sensors, is to be able to obtain a calibration coefficient at an equilibrium without needing the system to reach it. The calibration coefficient of a sensor j against a reference R can be defined as

$$c_{jR} = \frac{y_{\infty_R}}{y_{\infty_j}} \tag{1}$$

where y_{∞_j} and y_{∞_R} are the asymptotic value of the readout of a sensor j and reference R at equilibrium, respectively. A sensor can, in the s-domain, be modeled as a first order transfer function, $H_j(s) = Y(s)/X(s)$, where $Y(s)$ is the output of the sensor (readout) and $X(s)$ is the input (measurand). By applying the inverse Laplace transform to return to the time domain and taking the limit as $t \to \infty$, the asymptotic value can be obtained [29]

$$y_{\infty_j} = \lim_{t\to\infty} \mathcal{L}^{-1}\left[H_j(s)\right] = \frac{k_j z_j}{p_j} \tag{2}$$

resulting in

$$c_{jR} = \frac{y_{\infty_R}}{y_{\infty_j}} = \frac{\frac{k_R z_R}{p_R}}{\frac{k_j z_j}{p_j}} \tag{3}$$

In a sensor network, the sensor specific transfer function $H(s)$ is not possible to obtain from the raw data due to the input $X(s)$ not being defined. This issue can be avoided by obtaining the calibration coefficient by starting with the overall transfer function $H_{ij}(s)$ between two sensors i and j, where the

Table 1. Summary table of general information of the two sensor networks used. Note that the number of sensors also include the network reference sensor. 0 sensors indicate zero successfully calibrated sensors.

	Helsinki			Antwerp		
Quantity	Sensors	Frequency	Limitations	Sensors	Frequency	Limitations
Temp.	7	1 h	Low frequency	7	1 min	None
RH	7	1 h	Low frequency	7	1 min	None
Pressure	7	1 h	Low frequency	7	1 min	None
PM_{10}	0	1 h	Readouts too low	4	1 min	Localized readouts
$PM_{2.5}$	0	1 h	Readouts too low	4	1 min	Localized readouts

medium effect is present, and the input is the readout of sensor i and the output the readout of sensor j. By denoting the output of a sensor for a quantity as Q, the following can be derived:

$$\begin{aligned} H_{ij}(s) &= \frac{Q_j(s)}{Q_i(s)} \\ H_{ij}(s) &= \frac{Q_{j_{\text{real}}}(s)\,H_j(s)}{Q_{i_{\text{real}}}(s)\,H_i(s)} \\ H_{ij}(s) &= H_{ij}^{\text{M}}(s)\,\frac{H_j(s)}{H_i(s)} \\ \frac{H_{ij}(s)}{H_{ij}^{\text{M}}(s)} &= \frac{H_j(s)}{H_i(s)} \end{aligned} \tag{4}$$

where $H_{ij}^{\text{M}}(s)$ is the first order medium transfer function between sensors i and j, $H_j(s)$ and $H_i(s)$ are the sensor specific transfer functions, $Q_{j_{\text{real}}}$ and $Q_{i_{\text{real}}}$ the actual value of the measurand at the sensor positions, and Q_j and Q_i the readouts of the same measurand. Equation (4) shows that the transfer function $H_j(s)/H_i(s)$ is equal to removing the medium effect $H_{ij}^{\text{M}}(s)$ from the overall transfer function $H_{ij}(s)$. By applying the same operations as in equation (2) on the left side of equation (4), the calibration coefficient can be obtained:

$$\frac{k_{ij}z_{ij}p_{ij}^{\text{M}}}{k_{ij}^{\text{M}}z_{ij}^{\text{M}}p_{ij}} \approx \frac{k_{ij}}{k_{ij}^{\text{M}}} = c_{ij} = \frac{y_{\infty_j}}{y_{\infty_i}} \tag{5}$$

where it has been assumed that the medium effects z_{ij}^{M} and p_{ij}^{M} are negligible, and therefore, equal to 1. It has also been assumed that the variety in sensor specific zeros and poles is minimal, hence the fraction containing the overall parameters z_{ij}/p_{ij} cancels itself out. These assumptions are expected to be most valid when the sensor nodes are of comparable type, the measurand varies sufficiently smoothly over the network scale, and the selected time window provides sufficient correlation between sensor signals [26].

2.2. Data

Two different sensor networks were targeted for calibration. Different preprocessing were required for successful application of the method. The following subsection presents the datasets. Table 1 shows a summary containing general information of the two sensor networks.

2.2.1. Helsinki

The SMEAR III station supports multidisciplinary observations of aerosol dynamics, atmospheric chemistry, micrometeorology, meteorological parameters, and urban vegetation ecophysiology. Its unique characteristics include its high-latitude location and proximity to the Baltic Sea. The station is jointly operated by the University of Helsinki and the Finnish Meteorological Institute.

The station network consists of three sites representing different urban surface environments. The main site, located in the Kumpula campus area approximately four kilometers northeast of central Helsinki, is classified as semi-urban with heterogeneous surface cover including buildings, roads, and vegetation [30]. Micrometeorological measurements are conducted from a 31 m tower positioned on a rocky hill and include radiation measurements, air temperature, wind profiles, and turbulent fluxes of momentum, heat, water vapor, carbon dioxide (CO_2), and aerosol particle number using the eddy covariance technique. Additional campaigns focus on nitrous oxide and volatile organic compound fluxes.

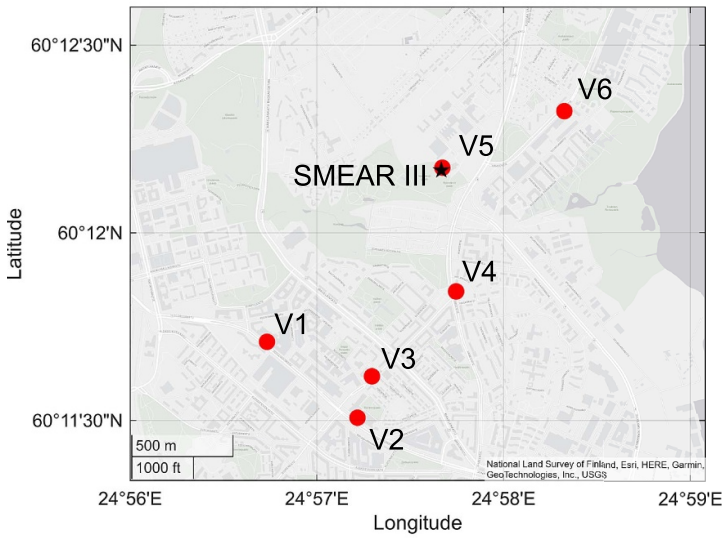

Figure 1. The Helsinki sensor network [14]. The black star marker is the SMEAR III station [15]. Reproduced from [26]. CC BY 4.0.

An adjacent air-conditioned container houses instrumentation for aerosol particle size distributions, chemical composition, and optical properties, together with trace-gas measurements. The station also operates a meteorological site on a University of Helsinki rooftop at 50 m height [31]. For this work, meteorological variables that include temperature, RH, and pressure from the SMEAR III station were used. The sensor used for measuring temperature is the Pt100, for RH HMP155, and for measuring pressure the Vaisala DPA502 was used.

At the SMEAR III station, supplementary air quality measurements were conducted using AQT530 (Air Quality Transmitter 530, Vaisala Ltd) sensors in addition to existing observational infrastructure. The study aimed to (i) characterize the performance of the AQT530 laser-based particle counters under controlled laboratory conditions, with emphasis on detection efficiency as a function of particle size and number concentration using monodisperse aerosols, (ii) evaluate long-term sensor performance through co-location with reference-grade instrumentation for gaseous and particulate pollutants at an air quality monitoring site, and (iii) assess the utility of a distributed network of 25 sensor units (AQT560 [32]) deployed across the Helsinki metropolitan area for capturing spatial and temporal variability associated with long-range transport events, local emission hotspots, and road dust episodes [14]. For this work, temperature, RH, and pressure values from these sensors in the Valilla area were used. PM_{10} and $PM_{2.5}$ were not possible to use due to too low values of the quantity in the area, resulting in unsuccessful generation of feasible transfer functions. The sensor locations are shown in figure 1.

The frequency of the sensors (except for the reference) was 1 hour (figure 2), which is not sufficient for finding the required correlation between the readings for transfer function generation. This was solved by applying a polynomial smoothing spline using MATLAB's fitting tool on the raw data, increasing the frequency of data points to one per min. This solution may decrease the validity of the data due to the number of generated data points and should be used with caution. Extremely dynamic quantities cannot be preprocessed using this approach, however, temperature, RH, and pressure are quantities that usually do not show erratic behavior in this time range in a city environment. To obtain the overall transfer function, $H_{ij}(s)$, with physically feasible k_{ij} and small enough uncertainties, the data was submitted to an algorithm screening through different segments of the data. The time frame of the segment was chosen as $5h$ to have a sufficient long time range to capture the behavior of the signals but not too long to lose correlation between the start and the end of the measurement. It is worth noting that the choice of the segment is not fixed; it should be chosen based on an understanding of the physical behavior of the system and evaluation of the parameters of the obtained transfer functions.

2.2.2. Antwerp

This dataset consisted of a large number of sensors spread around Antwerp and is part of a large European city monitoring project: SensEURCity. In the cities (Antwerp, Oslo, Zagreb), the sensors that

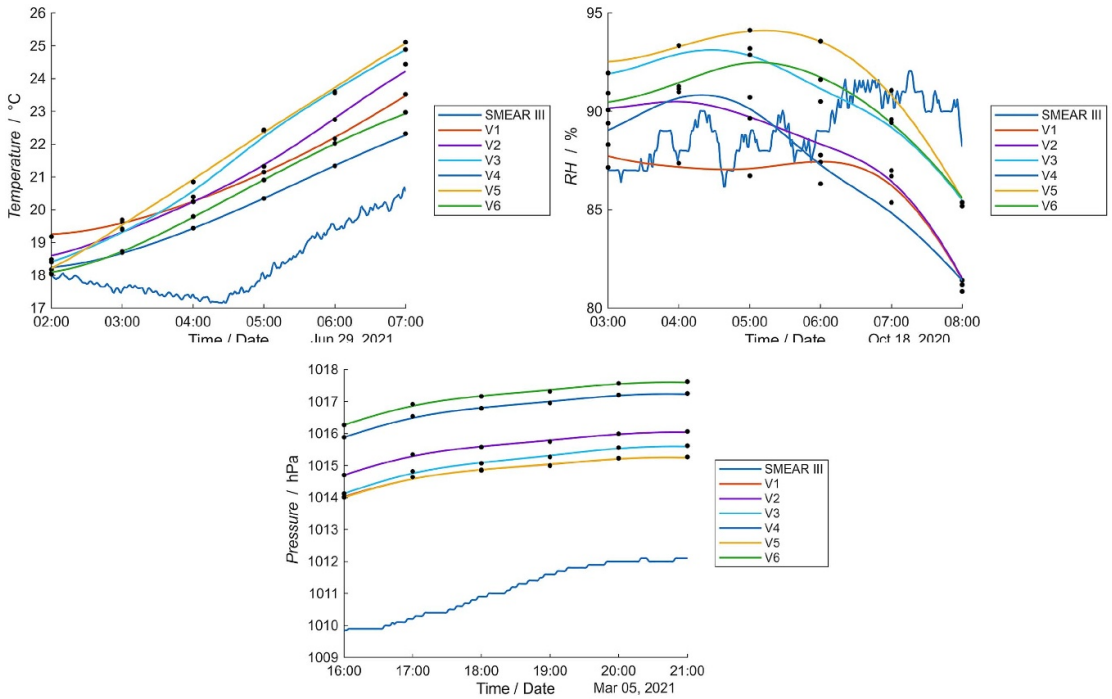

Figure 2. Post-processed data from the Helsinki sensor network. The black dots represent the raw data points for the sensors under calibration. The reference has a measurement frequency of 1 min, and hence, its raw data points are not plotted. The pressure curve for V1 lies under V5.

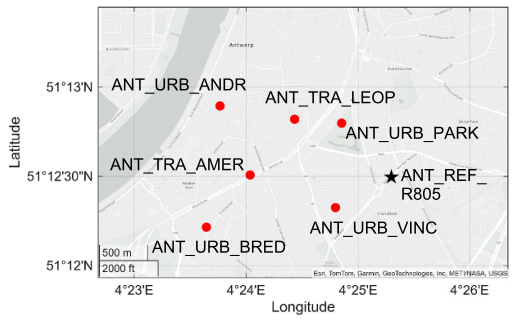

Figure 3. The sensors used in the Antwerp network. The red dots mark sensors that were calibrated using the method, while the black star is the network reference station R805.

were targeted for calibration, have three different stages: first co-location, deployment, and second co-location. For the calibration, we have only taken data points from the deployment stage, since that corresponds the best to a real-world case [24]. Figure 3 shows the location of the sensors targeted for calibration.

The reference station R805, which is located in Belgiëlei, was chosen to act as the network reference. While live-data for temperature, RH, and pressure can be obtained from this station, information regarding the used equipment is not available, and therefore, the repeatability to be propagated for these measurands were chosen to be the same as that of the devices under calibration. For the monitoring of PM_{10} and $PM_{2.5}$ at this location, the Pala Fidas 200 is used, which has a repeatability of 3 % [33]. The temperature and RH sensors targeted for calibration were Sensirion SHT31TE and SHT31HE [34], respectively, and pressure is measured by Bosch BMP280 [35]. The PM measurements were conducted with Alphasense—OPC-N3 sensors [36].

The frequency of all sensors in this dataset was 1 min (figure 4). A smoothing spline was also applied to this dataset, however, points between timestamps were not used for generation of the transfer functions. In this dataset it was possible to calibrate the sensors for temperature, RH, pressure, PM_{10}, and $PM_{2.5}$. However, due to lack of correlation between some sensors, a smaller number of sensors where used in calibration of the PM measurements.

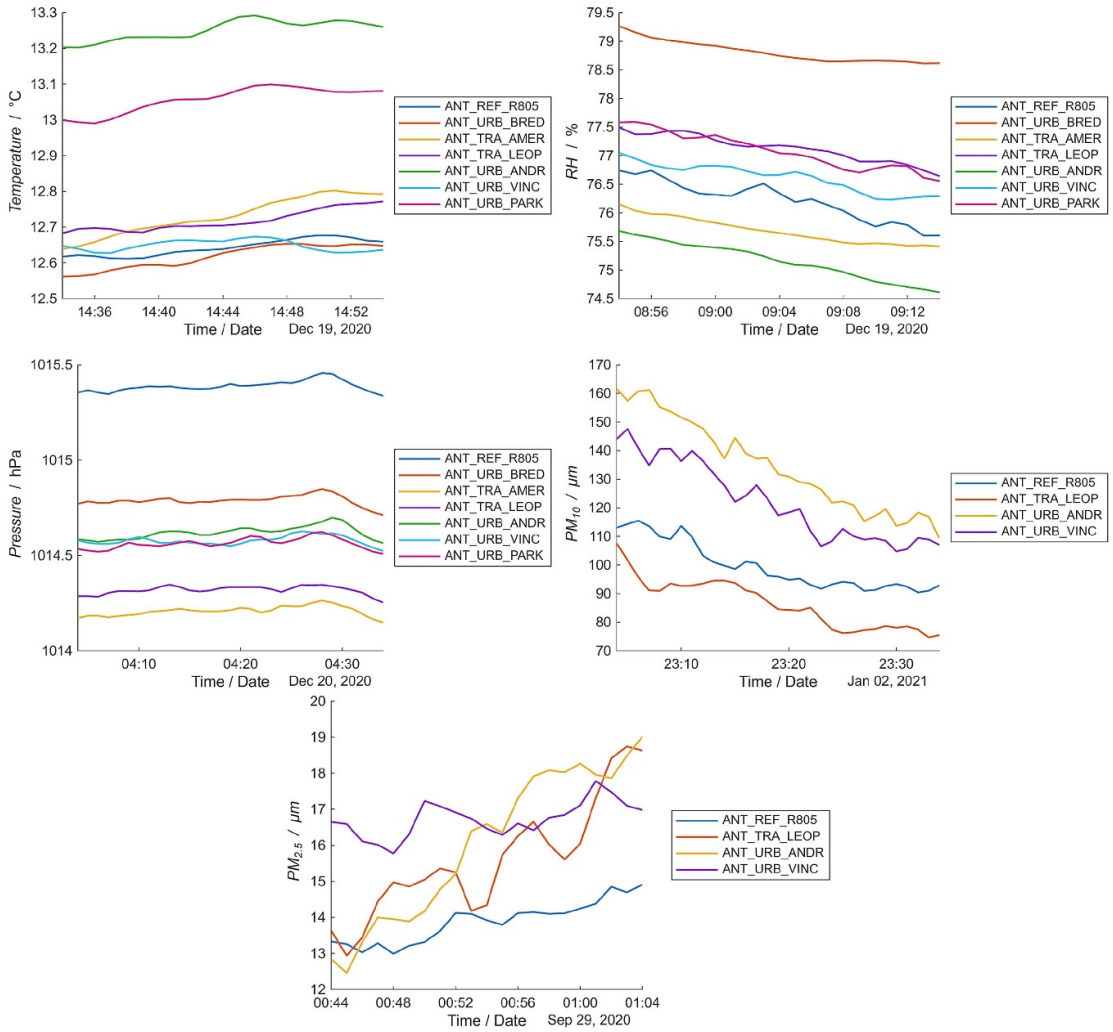

Figure 4. Post-processed data from the Antwerp sensor network. The measurement frequency of all sensors is 1 min.

2.3. Algorithm

Transfer functions were estimated for all feasible sensor pairs within selected time windows. Fits with unstable poles, non-physical gain values, poor convergence, or excessive gain uncertainty were rejected. Figure 5 shows the algorithm process.

In the third step, the order of the fitting depends on the sensor network under study. In a real-world sensor network, all sensors have an x and an y coordinate, which would result in a 4th order polynomial. However, by instead applying the fitting on the spatial differences between two sensors, the order of the polynomial can be reduced to two. This fitting then corresponds to the medium effect $H_{ij}^{\mathrm{M}}(s)$, which is separated from the overall transfer function $H_{ij}(s)$.

During the Monte Carlo algorithm, the uncertainties $u(k_{ij})$, $u(\hat{k}_{ij}^{\mathrm{M}})$, and $u(c_{rR})$ need to be propagated [37]. The uncertainty $u(k_{ij})$ is the combined uncertainty of the uncertainty of k_{ij} obtained from the estimation of $H_{ij}(s)$ and the repeatability of the measurement. The uncertainty of $u(\hat{k}_{ij}^{\mathrm{M}})$ is the standard deviation of $\hat{k}_{ij}^{\mathrm{M}}$ when calculating the fitting with $u(k_{ij})$, and $u(c_{rR})$ is the repeatability of the reference.

The target of the calibration is the calibration coefficient c_{jR}, which means sensor j calibrated against a reference R. The matrix $\mathbf{c}_{ij}$ consists of calibration coefficients whose definition is sensor i calibrated against sensor j. These coefficients do not correspond to a calibrated sensor (both i and j are uncalibrated), hence the equation $c_{iR}/c_{jR} - k_{ij}/\hat{k}_{ij}^{\mathrm{M}} = 0$ is needed to obtain c_{jR}.

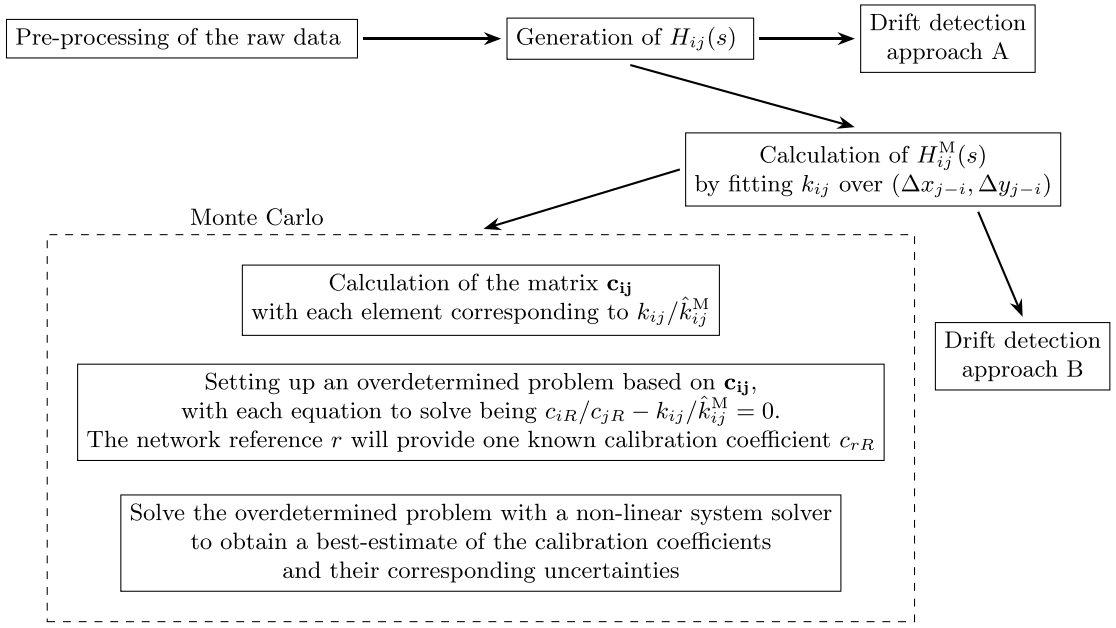

Figure 5. The full workflow of the Laplace-domain method and where its drift detection is applied.

3. Drift detection

To further add to the functionality of the method, we investigated whether changes in the pairwise transfer function structure can be used as indicators of sensor malfunction or drift. Identifying drifting sensors is not only important for the sake of obtaining correct measurement values; this method heavily depends on the sensors exhibiting a non-drifting behavior to ensure a valid calibration. In this work, the approach is evaluated using artificially introduced multiplicative shifts. The results should therefore be interpreted as sensitivity tests for synthetic malfunction scenarios rather than as full validation against real long-term sensor drift. However, by performing multiple calibrations on a set of sensors in a network over a longer time span, it would be possible to outline if a drift is present in the sensors. The two proposed approaches are as following:

A. Comparison of current k_{ij} with past k_{ij}.

B. Calculating the difference in $\hat{k}_{ij}^{\mathrm{M}}$ with a sensor omitted and with the sensor present.

Approach A is mathematically simpler than approach B, however, it requires the storage of historical k_{ij}. Therefore, approach B is more feasible in real-time detection of drifting sensors. It should be noted that since it is based on the changes in the fitting, only sensors central in the sensor network should be checked with this approach, since sensors located at the edges of the network may influence the fitting noticeably even without a present drift.

3.1. Approach A

When obtaining the overall transfer function, $H_{ij}(s)$, k_{ij} can be stored in a matrix of the form

$$\mathbf{k}_{ij} = \begin{bmatrix} 0 & k_{12} & k_{13} & \cdots & k_{1n} \\ 0 & 0 & k_{23} & \cdots & k_{2n} \\ \vdots & \vdots & \ddots & \ddots & \vdots \\ 0 & 0 & 0 & \cdots & k_{(n-1)n} \end{bmatrix} \tag{6}$$

where the row (first subscript) denotes the input sensor, and the column (second subscript) denotes the output sensor. If the readout of a sensor is shifted with a factor λ, a change can be seen in $\mathbf{k}_{ij}$. For

example, if sensor 3 is shifted with a factor λ, equation (6) will show an approximate change as:

$$\mathbf{k}_{ij} = \begin{bmatrix} 0 & k_{12} & \lambda k_{13} & k_{14} & \cdots & k_{1n} \\ 0 & 0 & \lambda k_{23} & k_{24} & \cdots & k_{2n} \\ 0 & 0 & 0 & \frac{1}{\lambda} k_{34} & \cdots & \vdots \\ \vdots & \vdots & \vdots & \ddots & \ddots & \vdots \\ 0 & 0 & 0 & 0 & \cdots & k_{(n-1)n} \end{bmatrix} \tag{7}$$

and therefore, it is possible to detect a sensor that has started to drift.

3.2. Approach B

Approach B is based on more sophisticated mathematics compared to Approach A. The core idea of the approach is to investigate the difference in $\hat{k}_{ij}^{\mathrm{M}}$ at a specific sensor location when said sensor is present in generation of the fitting and when it is not. We denote the difference for a drifted sensor λ as:

$$\Delta\hat{k}_{\lambda}^{\mathrm{M}} = \frac{1}{\lambda}\sum_{i=r}^{\lambda-1}\Delta\hat{k}_{i\lambda}^{\mathrm{M}} + \frac{1}{n-\lambda}\sum_{j=\lambda+1}^{n}\Delta\hat{k}_{\lambda j}^{\mathrm{M}} \tag{8}$$

which is the average value of the difference for each sensor pair where sensor λ is present either as input or output. The two differences in equation (8) are calculated as:

$$\begin{aligned} \Delta\hat{k}_{i\lambda}^{\mathrm{M}} &= |\hat{k}_{ij:i,j\neq\lambda}^{\mathrm{M}}(\Delta x_{i\lambda}, \Delta y_{i\lambda}) - \hat{k}_{ij}^{\mathrm{M}}(\Delta x_{i\lambda}, \Delta y_{i\lambda})| \\ \Delta\hat{k}_{\lambda j}^{\mathrm{M}} &= |\hat{k}_{ij:i,j\neq\lambda}^{\mathrm{M}}(\Delta x_{\lambda j}, \Delta y_{\lambda j}) - \hat{k}_{ij}^{\mathrm{M}}(\Delta x_{\lambda j}, \Delta y_{\lambda j})| \end{aligned} \tag{9}$$

In equation (9), $\hat{k}_{ij:i,j\neq\lambda}^{\mathrm{M}}$ is the fitted medium effect $H_{ij}^{\mathrm{M}}(s)$ without using either $k_{\lambda j}$ or $k_{j\lambda}$. The Δk of other central, local and non-drifted sensors is calculated in the same manner using equation (8), with λ changing to the corresponding non-drifted sensor indexes. The largest Δk should be obtained when equation (8) is calculated with sensor λ, and hence, the drifted sensor can be detected.

Equation (9) is the difference between the two fittings at the corresponding sensor location and it is valid to ask why it is not sufficient to only investigate the residuals between k_{ij} and $\hat{k}_{ij}^{\mathrm{M}}$, since k_{ij} of a shifted sensor should have the largest residual to $\hat{k}_{ij}^{\mathrm{M}}$. While this is true, and that approach showed promise, the ratio $\Delta k_{i\neq\lambda}/\Delta k_{\lambda}$ is smaller (easier to spot the malfunctioning sensor) when using equation (9). This is most likely due to the residual calculation of $\Delta k_{i,j\neq\lambda}$ always containing at least one k_{ij} that is affected by the shifted sensor, either with sensor λ as the input or output, while equation (9) uses $\hat{k}_{ij:i,j\neq\lambda}^{\mathrm{M}}$, where the shifted sensor's effect is not present.

4. Results & discussion

This section presents the obtained calibrations with the method. The best-estimates of the calibration coefficients are plotted with an uncertainty of two standard deviation (coverage factor = 2) and a shaded area in the plots that denotes the uncertainty reported by the manufacturer or other specification if said otherwise. Comparison with the specifications is useful as a practical benchmark: it indicates that calibration can provide measurements with lower uncertainty during the evaluated period than would be assigned using the specifications alone. It does not demonstrate that this lower uncertainty remains valid over the full period covered by the specifications. A comparison with conventional calibration results under equivalent conditions would be more direct, but such results were unavailable. The drift detection results are included under their corresponding datasets.

4.1. Helsinki

In the Helsinki sensor network, we obtained calibration coefficients for temperature, RH, and pressure. It was not possible to obtain feasible transfer functions for PM_{10} and $PM_{2.5}$ between sensors in this area, which was most likely due to the low pollution levels in Helsinki, resulting in mostly noise in the signals and not a valid correlation between the readouts.

Table 2. The $\Delta\hat{k}_{\lambda}^{\mathrm{M}}$ for different sensors being shifted by 30 %. Bold values indicate the highest difference.

	Temperature			Relative Humidity			Pressure		
Shifted	V3	V4	V5	V3	V4	V5	V3	V4	V5
V3	**0.0462**	0.0156	0.0006	**0.0564**	0.0209	0.0118	**0.0507**	0.0160	0.0048
V4	0.0205	**0.0466**	0.0050	0.0128	**0.0439**	0.0070	0.0179	**0.0482**	0.0014
V5	0.0014	0.0027	**0.0535**	0.0073	0.0075	**0.0673**	0.0018	0.0025	**0.0598**

The best-estimates of the calibration coefficients (left side figure 6) for RH and pressure are at a maximum approximately two and one standard deviations from the assumed manufacturer value of 1, respectively. The uncertainties are lower than that of the specifications, except for sensor V1 for RH. The extremely low uncertainties for pressure are most likely a contribution of the small deviations in k_{ij}, which is a result of the low numerical difference in pressure between the sensors, and the stable nature of pressure as a phenomenon in an area of the size of this sensor network. The small deviations in the pressure calibration coefficients still indicates that the system has been modeled according to the present physics, and that the sensors do not experience the exact same dynamic conditions. The results of the temperature calibration differ more than that of the other quantities, which may be a result of the difference in the readouts between the sensors under calibration and the reference (figure 2). Two temperature calibration coefficients lie outside the manufacturer specification band. This may indicate weaker correlation with the reference, stronger local temperature effects, or limitations introduced by the interpolation and selected time window. In addition, if the reference station is not sufficiently representative of the local temperature field experienced by the sensor nodes, co-calibration among the sensors may provide a more appropriate basis for assessing their relative consistency than direct calibration against a single reference value.

The results of the drift detection can be seen from the right side of figure 6. It is evident that the value $\Delta\hat{k}_{i}^{\mathrm{M}}$ is the highest when omitting the drifted sensor from the fitting of $\hat{k}_{ij}^{\mathrm{M}}$, showing that it affects the fitting the most, and hence, is most likely the sensor exhibiting a drift. It is important to note that this approach should only be used when studying sensors central in the network. An edge sensor might affect the fitting noticeably even if it is not drifting, since its location will ensure it having a large weight on the fitting result. In table 2, $\Delta\hat{k}_{\lambda}^{\mathrm{M}}$ can be seen for sensors V3–V5 for temperature, RH, and pressure. It can be seen that Approach B detects the correct sensor when any of these sensors are shifted.

4.2. Antwerp

In the Antwerp sensor network, we obtained calibration coefficients for temperature, RH, pressure, PM_{10}, and $PM_{2.5}$. Due to PM size readings being an extremely localized phenomenon [10], it was required to reduce the number of sensors under calibration from six to three to obtain feasible transfer functions $H_{ij}(s)$ between sensors.

In this calibration (figure 7), the best-estimates for all measurands are inside the specifications of the sensors and further compared to Helsinki results (figure 6), the uncertainties also seem to generally be of lower magnitude. This is most likely due to the fitting $\hat{k}_{ij}^{\mathrm{M}}$ being of higher quality for the quantities in this network, which may be a result of better correlation between sensors. While a better correlation can be dependent on how localized the physical phenomenon is, it might in this case be attributed to the higher measurement frequency, resulting in no interpolated points being used between measurement points, and hence, better quality data to capture the correlation between sensor readouts. The uncertainty levels, except for PM_{10}, are all a noticeable improvement to the specifications.

The PM sensor calibrations show that the modeling of the system is successful and that the overdetermined problem can be solved (to an enough accurate level) for selected sensor subsets. However, for PM_{10} it is evident that the uncertainty starts to propagate noticeable for the third sensor, which is a result of the reduced number of usable sensors and the larger propagated uncertainties. This shows that PM is a more challenging measurand for this approach. Worth noting that the manufacturer uncertainty for these sensors has been assumed to be 15 %, which is in agreement with studies of uncertainty in PM-sensors, although thorough metrological evaluation of such sensors are lacking in literature.

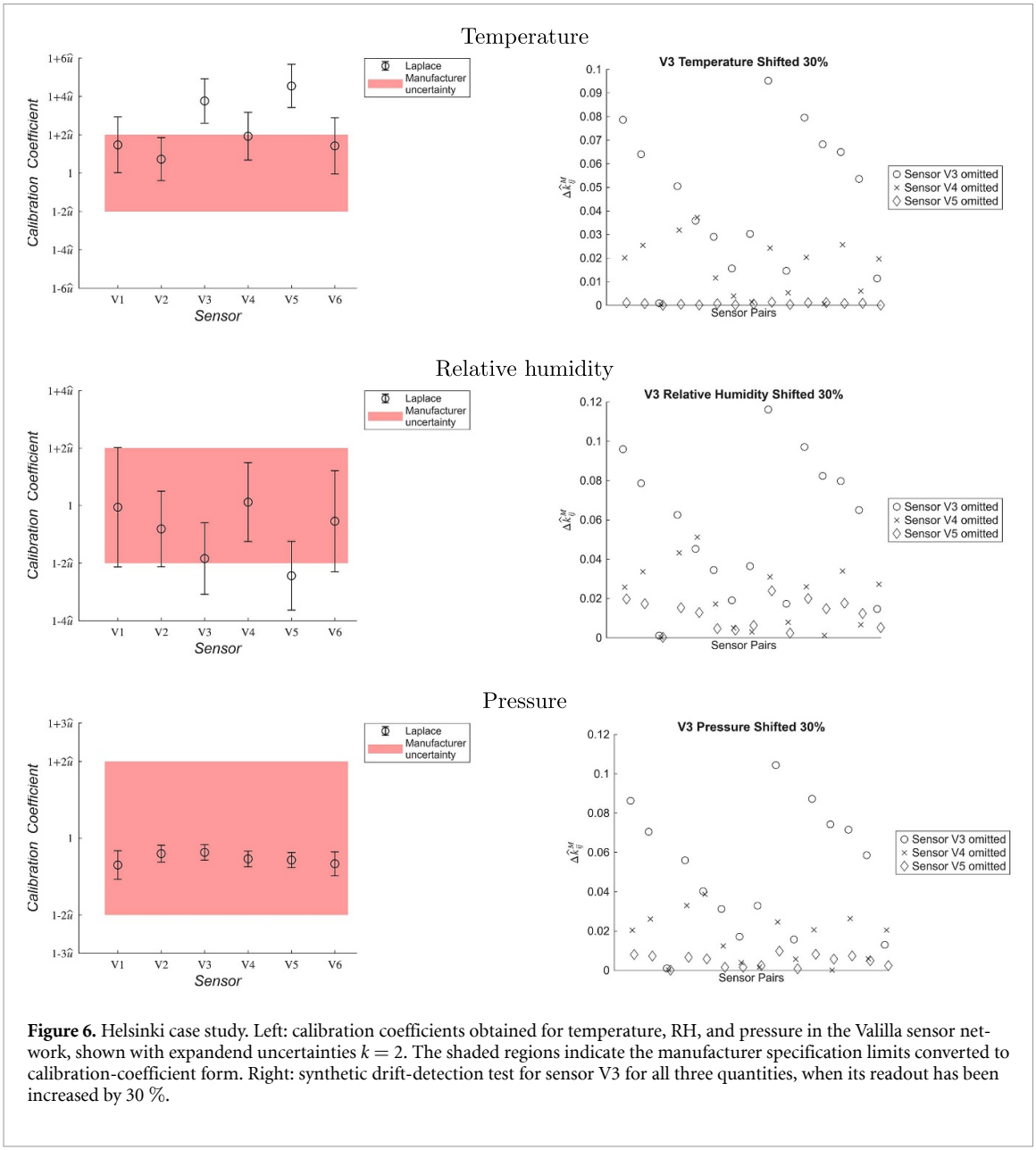

Figure 6. Helsinki case study. Left: calibration coefficients obtained for temperature, RH, and pressure in the Valilla sensor network, shown with expandend uncertainties $k = 2$. The shaded regions indicate the manufacturer specification limits converted to calibration-coefficient form. Right: synthetic drift-detection test for sensor V3 for all three quantities, when its readout has been increased by 30 %.

Table 3. The $\Delta\hat{k}_{\lambda}^{\mathrm{M}}$ for different sensors being shifted by 30 %. Bold values indicate the highest difference.

	Temperature			Relative Humidity			Pressure		
Shifted	LEOP	VINC	PARK	LEOP	VINC	PARK	LEOP	VINC	PARK
LEOP	**0.0456**	0.0074	0.0202	**0.0526**	0.0021	0.0182	**0.0501**	0.0045	0.0225
VINC	0.0060	**0.0650**	0.0037	0.0018	**0.0607**	0.0024	0.0012	**0.0629**	0.0058
PARK	0.0257	0.0066	**0.0632**	0.0177	0.0122	**0.0633**	0.0203	0.0093	**0.0591**

The drift detection was applied in the same manner for this network as with the Helsinki sensor network. In figure 7 it is clear that when omitting the drifted sensor (30 % increase) the value of $\Delta\hat{k}_{i}^{\mathrm{M}}$ is the largest, showing that the method is able to detect the drifting sensor. In table 3 the values of $\Delta\hat{k}_{\lambda}^{\mathrm{M}}$ can be found for sensors LEOP, VINC, and PARK when shifted for temperature, RH, and pressure.

For the PM approach B was not suitable to detect drifted sensors. This is most likely due to the low number of sensors, resulting in a large $\Delta\hat{k}_{j}^{\mathrm{M}}$ when omitting a non-drifted sensor, since omitting any sensor will affect the fitting noticeably. Approach A is still applicable, because the change in k_{ij} can be seen.

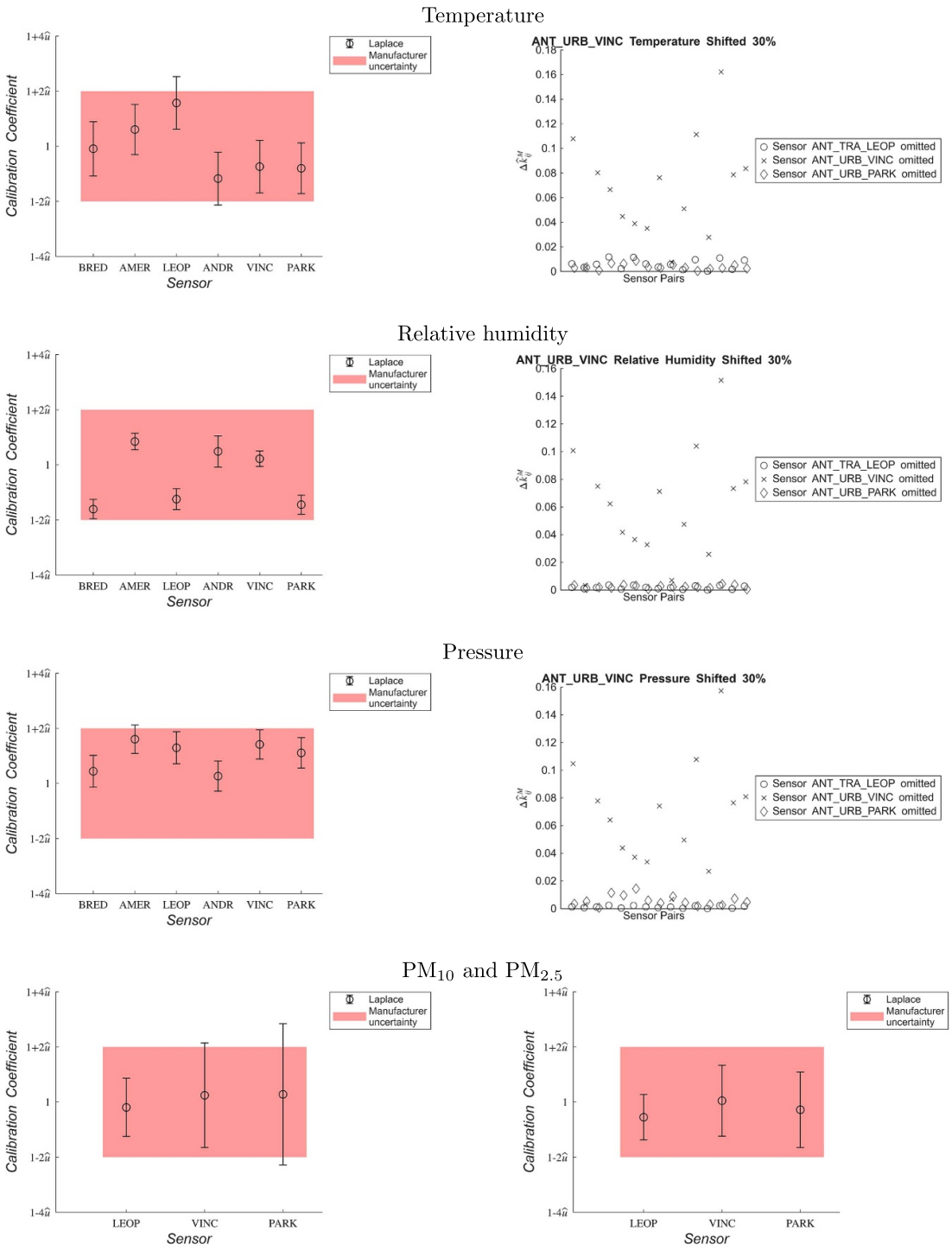

Figure 7. Antwerp case study. Left: calibration coefficients obtained for temperature, relative humidity pressure, PM_{10}, and $PM_{2.5}$ (right), shown with expanded uncertainties $k = 2$. The shaded regions indicate manufacturer specification limits converted to calibration-coefficient form. Right: synthetic drift-detection for sensor VINC for temperature, RH, and pressure when its readout has been increased by 30%.

5. Conclusion

This paper has presented a Laplace-domain calibration method and its applicability for calibration of sensors in two different real-world city-scale sensor networks, one stationed in Helsinki and one in Antwerp. The method obtains transfer functions between readouts of the sensors to model the combination of present medium physics and sensor behavior in the network, from which the medium effect can be modeled. By separating this effect, the method calculates calibration coefficients dependent only on the intrinsic sensor behavior. In both sensor networks the obtained calibration coefficients for the

sensors under calibration for temperature, RH, and pressure, show an improvement after calibration when comparing to the specifications provided by the manufacturer. This points to the method achieving in modeling the physics present in the network and successfully separating the medium effect.

Calibration for particulate matters PM_10 and $PM_2.5$ was not possible in the Helsinki network, due to the pollution level being too low. In the Antwerp network, the calibration yielded positive results for a subset of sensors, however, the need of reducing the number of sensors under calibration shows that calibration of localized phenomena such as PM pollution level requires investigation of the correlation between sensors. It can be assumed that the method should work for other air pollutants as long as correlation between sensors is strong enough, i.e. the behavior of the pollutant is not too localized at sensor positions in the network, since the method is not dependent on the unit of the quantity but its behavior.

The method also allows for drift detection and two different approaches have been outlined: comparison of historical and present transfer function constant parameters, and omission of sensors in medium effect modeling for investigation of medium effect differences. The approaches have been tested by shifting sensors in the network for detection, and the first approach showed to be viable for all quantities. The more complex second approach worked for temperature, RH, and pressure in both networks, however, it did not yield successful detection for PM measurements. This is, however, most likely due to the small number of sensors present in the calibration, and not a limitation directly linked to the quantity itself.

Other limitations would include high noise levels and significant heterogeneity. High noise would result in the modeling of the medium to be more challenging, which would lead to higher uncertainties in $\hat{k}_{ij}^{M}$, resulting in a larger uncertainty being propagated in the algorithm. Significant heterogeneity in the network may influence the quality of the generated transfer functions between the sensors, since their response times may be different. This might require higher grade transfer functions to take this phenomenon into consideration, which would demand investigation of the medium effect on zeros and poles, and if observed, also propagated through the algorithm.

This study shows that this method could be a reasonable alternative to conventional methods for calibration of sensors in a city-wide sensor network for both generally non-localized phenomena and more localized phenomena. Furthermore, other types of sensor networks, e.g. IoT (internet of things) networks or smart cities, could also be suitable for calibration by this method, provided that the medium effect can be modeled in the network. Correlation issues between sensors in a spatially wide network for localized quantities are an aspect that would benefit of further research, and if solutions would be found, it would not only result in a larger number of calibrated sensors, but also in lower obtained uncertainties for the sensors under calibration thanks to the redundancy of the system becoming greater.

Acknowledgment

The project (22DIT02 FunSNM) has received funding from the European partnership on metrology, co-financed from the European union's Horizon Europe Research and Innovation Programme and by the participating states, and through Research Council of Finland via the Atmosphere and Climate Competence Center (374287), INAR RI (358647, 367739) and research projects (370556). The authors would like to thank Jarkko V. Niemi and Hanna Manninen from the Helsinki Region Environmental Services (HSY), as well as Hilkka Timonen from the Finnish Meteorological Institute (FMI), for providing the reference air quality data used in this study.

Data availability statement

The data that support the findings of this study are available upon reasonable request from the authors.

The Antwerp dataset can be found online https://zenodo.org/records/17858205, and the Helsinki data is not publicly accessible but is available by request by the authors in https://www.frontiersin.org/journals/environmental-science/articles/10.3389/fenvs.2021.719 567/full#s2. The data to obtain the results and the results will be made available upon request. The reason to not make it available at the moment is the lack of resources (project has ended).

Declaration of generative AI and AI-assisted technologies in the writing process

During the preparation of this work, some of the authors used ChatGPT by OpenAI for English grammar correction, language polishing, and readability checks. After using this tool, the authors reviewed and edited the content as needed and take full responsibility for the content of the published article.

Author contributions

Henrik Söderblom 0009-0005-5549-302X
Conceptualization (lead), Formal analysis (lead), Software (lead), Validation (lead), Visualization (lead), Writing – original draft (lead)

Martha A Zaidan 0000-0002-6348-1230
Data curation (equal), Writing – review & editing (equal)

Maitane Iturrate-Garcia 0000-0002-1517-3305
Writing – review & editing (equal)

Hasan Sarwar 0009-0009-4939-2416
Data curation (equal), Writing – review & editing (equal)

Richard Högström 0000-0002-1718-1149
Writing – review & editing (equal)

Tuukka Petäjä 0000-0002-1881-9044
Data curation (equal), Writing – review & editing (equal)

Shahin Tabandeh 0009-0005-3936-4519
Funding acquisition (lead), Methodology (lead), Project administration (lead), Supervision (lead), Writing – review & editing (lead)

References

[1] WHO, Health effects of air pollution – evidence and implications: technical brief, Technical Report, World Health Organization (WHO Air Quality, Energy and Health Science and Policy Summaires), 2026 (https://doi.org/10.2471/B09563)
[2] Rai M *et al* 2023 Heat-related cardiorespiratory mortality: effect modification by air pollution across 482 cities from 24 countries *Environ. Int.* **174** 107825
[3] Stafoggia M *et al* 2023 Joint effect of heat and air pollution on mortality in 620 cities of 36 countries *Environ. Int.* **181** 108258
[4] Kampa M and Castanas E 2008 Human health effects of air pollution *Environ. Pollut.* **151** 362–7
[5] Manisalidis I, Stavropoulou E, Stavropoulos A and Bezirtzoglou E 2020 Environmental and health impacts of air pollution: A review *Front. Public Health* **8:14** 14
[6] Kim E E, Kang J, Su J and Lee S J 2026 The relationship between all-cause mortality and air pollution: a systematic review focusing on vulnerable populations *Air Qual. Atmos. Health* **19** 145
[7] Elbestar M, Aly S G and Ghannam R 2024 Advances in air quality monitoring: a comprehensive review of algorithms for imaging and sensing technologies *Adv. Sens. Res.* **3** 2300207
[8] Aini Q, Manongga D, Rahardja U, Sembiring I and Li Y-M 2025 Understanding behavioral intention to use of air quality monitoring solutions with emphasis on technology readiness *Int, J. Hum.–Comput. Interact.* **41** 5079–99
[9] Sangkham S, Phairuang W, Sherchan S P, Pansakun N, Munkong N, Sarndhong K, Islam M A and Sakunkoo P 2024 An update on adverse health effects from exposure to pm2. 5 *Environ. Adv.* **18** 100603
[10] Wang A, Paul S, Desouza P, Machida Y, Mora S, Duarte F and Ratti C 2023 Key themes, trends and drivers of mobile ambient air quality monitoring: a systematic review and meta-analysis *Environ. Sci. Technol.* **57** 9427–44
[11] Karagulian F *et al* 2019 Review of the performance of low-cost sensors for air quality monitoring *Atmosphere* **10** 506
[12] Snyder E G *et al* 2013 The changing paradigm of air pollution monitoring *Environ. Sci. Technol.* **47** 11369–77
[13] Morawska L *et al* 2018 Applications of low-cost sensing technologies for air quality monitoring and exposure assessment: How far have they gone? *Environ. Int.* **116** 286–99
[14] Petäjä T *et al* 2021 Added value of vaisala aqt530 sensors as a part of a sensor network for comprehensive air quality monitoring *Front. Environ. Sci.* **9** 719567
[15] Zaidan M A *et al* 2020 Intelligent calibration and virtual sensing for integrated low-cost air quality sensors *IEEE Sens. J.* **20** 13638–52
[16] Spinelle L *et al* 2015 Field calibration of a cluster of low-cost available sensors for air quality monitoring. part a: Ozone and nitrogen dioxide *Sens. Actuators B* **215** 249–57
[17] Spinelle L *et al* 2017 Field calibration of a cluster of low-cost commercially available sensors for air quality monitoring. part b: No, co and co2 *Sens. Actuators B* **238** 706–15
[18] Mai C *et al* 2025 Field-based calibration and operation of low-cost sensors for particulate matter by linear and nonlinear methods *Atmos. Pollut. Res.* **16** 102676
[19] Sousan S *et al* 2025 Advancing low-cost air quality monitor calibration with machine learning methods *Environ. Pollut.* **374** 126191

[20] Vajs I et al 2023 Data-driven machine learning calibration propagation in a hybrid sensor network for air quality monitoring *Sensors* **23** 2815
[21] Delaine F et al 2019 In situ calibration algorithms for environmental sensor networks: a review *IEEE Sens. J.* **19** 5968–78
[22] Gruber M et al 2023 Co-calibration in distributed homogeneous sensor networks *Proc. SMSI Nuremb. Ger.* **10** 47-8
[23] Eichstädt S and Werhahn O 2024 Metrology for sensor networks: metrological traceability and measurement uncertainties for air quality monitoring tm- *Tech. Mess.* **91** 419–29
[24] Van Poppel M 2023 Senseurcity: A multi-city air quality dataset collected for 2020/2021 using open low-cost sensor systems *Sci. Data* **10** 322
[25] De Vito S et al 2023 A global multiunit calibration as a method for large-scale iot particulate matter monitoring systems deployments *IEEE Trans. Instrum. Meas.* **73** 1–16
[26] Söderblom H et al 2026 A laplace-domain method for in situ temperature calibration in sensor networks *Meas.: Digit.* **6** 100025
[27] Harris P et al 2025 Measurement uncertainty evaluation for sensor network metrology *Metrology* **5** 3
[28] Järvi J 2009 The urban measurement station smear iii: continuous monitoring of air pollution and surface–atmosphere interactions in helsinki, finland *Boreal Environ. Res.* **14** 86
[29] Tabandeh S 2019 Advances in humidity standards *Ph.D. thesis*
[30] Fung P L et al 2021 Evaluation of white-box versus black-box machine learning models in estimating ambient black carbon concentration *J. Aerosol Sci.* **152** 105694
[31] Institute for Atmospheric and Earth System Research (INAR) 2026 *Smear iii station*
[32] Vaisala 2024 Air quality transmitter aqt560 (Accessed 2nd July 2026)
[33] Palas 2026 Pala fidas 200 instrument (Accessed 2 July 2026)
[34] Sensirion 2022 Datasheet sht3x-dis (Accessed 2 July 2026)
[35] Bosch 2021 Bmp280 - datasheet (Accessed 2 July 2026)
[36] Alphasense 2026 Opc-n3 particle monitor (Accessed 2 July 2026)
[37] J. C. for Guides in Metrology (JCGM), Evaluation of Measurement Data — Supplement 1 to the 'Guide to the Expression of Uncertainty in Measurement' — Propagation of Distributions Using a Monte Carlo Method, Technical Report BIPM, 2008